Global and Planetary Change 253 (2025) 104973

Contents lists available at ScienceDirect

Global and Planetary Change

journal homepage: www.elsevier.com/locate/gloplacha

Research Article

Diapycnal fluxes of nutrients in the North Pacific Subtropical Gyre☆

Chuanjun Du [a,b], Minhan Dai [a,*], Zhiyu Liu [a], Zhendong Hu [a], Jin-Yu Terence Yang [a], Kuanbo Zhou [a], Hongyang Lin [a], Zhongwei Yuan [a], Lifang Wang [a], Tao Huang [a], Liguo Guo [a], Zhe Wang [a], Shuh-Ji Kao [b]

[a] State Key Laboratory of Marine Environmental Science, College of Ocean and Earth Sciences, Xiamen University, Xiamen 361102, China
[b] School of Marine Science and Engineering & State Key Laboratory of Marine Resource Utilization in South China Sea, Hainan University, Haikou 570228, China

ARTICLE INFO

Editor Name: Dr. Sun Jimin

Keywords:
Diapycnal fluxes
Nutrients budget
North Pacific Subtropical Gyre

ABSTRACT

The supply of nutrients via diapycnal processes from depth to the euphotic zone (EZ) is thought to be a main source sustaining new production in oligotrophic oceans. However, such diapycnal fluxes of nutrients remain insufficiently constrained due to limited observations and the dynamic nature of ocean turbulence. In this study, we present a comprehensive dataset of diapycnal fluxes of nutrients, including diapycnal diffusive (F_{diff_NOx}) and effective diapycnal fluxes (F_{e_NOx}, representing the net diapycnal influx to the upper water column) of NO_3^- + NO_2^- (NO_x^-), based on measurements of turbulence microstructure and nutrients with high vertical resolutions from two cruises conducted during summer and winter in the oligotrophic western North Pacific Subtropical Gyre (NPSG). The F_{diff_NOx} (F_{e_NOx}) exhibits evident spatial variations, with higher values observed at the south boundary of the NPSG near the North Equatorial Current and at the northern NPSG influenced by the North Pacific Tropical Subtropical Mode Water. In contrast, lower values are found in the central NPSG. These spatial variations are primarily attributable to the vertical concentration gradient of NO_x^-. At the base of the EZ, the cruise-averaged F_{diff_NOx} (F_{e_NOx}) are 11.7 ± 9.6 (11.9 ± 8.6) and 8.5 ± 6.1 (11.3 ± 9.3) μmol m^{-2} d^{-1} in summer and winter, respectively, displaying insignificant seasonal variations. Moreover, we observed significantly higher flux ratios of F_{diff_NOx} to diapycnal diffusive flux of phosphate (F_{diff_DIP}), which were 18.2 ± 2.0 and 13.9 ± 2.0, compared to the N/P concentration ratios of 10.4 ± 1.1 and 7.4 ± 1.2 at the base of the EZ during summer and winter cruises, respectively, suggesting that the diapycnal transport could relieve nitrogen limitation in the upper NPSG. Notably, we identified strong linear relationships between the logarithm of F_{diff_NOx} (F_{e_NOx}) and the NO_x^- gradient. Leveraging these relationships, we estimate the climatological distributions of F_{diff_NOx} (F_{e_NOx}) utilizing nutrient data from the World Ocean Atlas (WOA23). The F_{e_NOx} is estimated to be 20.2 ± 16.6 μmol m^{-2} d^{-1} and contributes to 8.5 ± 8.3 % of the nitrogen required for new production in the NPSG. These estimates are slightly lower than previous studies, but highlight that diapycnal fluxes play a less important role on nitrogen budget compared to N_2-fixation and atmospheric deposition in the oligotrophic NPSG. In contrast, the effective diapycnal diffusive flux of phosphate (F_{e_DIP}) is 1.5 ± 1.3 μmol m^{-2} d^{-1}, contributing to 18.1 ± 17.9 % of the phosphorus required by new production, and is roughly ten times larger than the atmospheric phosphorus deposition in the NPSG.

1. Introduction

The nutrient cycling in oceanic and associated biotic reservoirs influences the rates of biological production and the structure of marine ecosystems (e.g., Arrigo, 2005). Within highly oligotrophic oceanic regions, the low levels of macronutrients, in particular nitrogen, have been identified as the primary limiting factor for phytoplankton growth (Browning and Moore, 2023). Therefore, the supply rate of nutrients from depth to the upper ocean plays a crucial role in regulating marine primary production, new production, and export production, which ultimately determines the efficiency of the marine biological carbon pump that largely influences the oceanic uptake of atmospheric CO_2 (Lipschultz et al., 2002; Johnson et al., 2010; Sigman and Hain, 2012; Dai et al., 2023).

☆ This article is part of a Special issue entitled: 'Western Pacific biogeochemical cycle' published in Global and Planetary Change.

* Corresponding author.
E-mail address: mdai@xmu.edu.cn (M. Dai).

https://doi.org/10.1016/j.gloplacha.2025.104973
Received 27 July 2024; Received in revised form 25 March 2025; Accepted 6 July 2025
Available online 8 July 2025

Among others, field measurements of turbulence combined with nutrient analysis offer a direct approach to effectively constrain the vertical transport of nutrients. This approach has been employed to investigate the nutrient supply to the upper ocean (e.g., Lewis et al., 1986; Kaneko et al., 2013; Painter et al., 2013; Fernández-Castro et al., 2015; Du et al., 2017; Hashihama et al., 2021). Recent global estimates indicate that nitrate diffusive fluxes are comparable to the sum of inputs from nitrogen fixation, fluvial fluxes, and atmospheric deposition (Mouriño-Carballido et al., 2021). Nonetheless, prior studies reveal a significantly large range in the estimates of diapycnal fluxes of nitrate, spanning from 0.007 to 42 mmol m^{-2} d^{-1}, across different oceanic regimes - a variation of up to four orders of magnitude (Mouriño-Carballido et al., 2021). Furthermore, each turbulence measurement captures processes spanning timescales from seconds to minutes (Liu and Lozovatsky, 2012), with the corresponding derived diapycnal flux representing an instantaneous value. These variations can mainly be ascribed to sparse observations, the dynamic nature of ocean turbulence, along with the spatial heterogeneity and vertical isopycnal displacements. All of these factors give rise to fluctuations in the estimates of nutrient fluxes. Consequently, accurately quantifying the diapycnal fluxes of nutrients into the euphotic zone (EZ) presents a considerable challenge.

The North Pacific Subtropical Gyre (NPSG) represents one of the largest surface marine biomes in the world's oceans (Karl and Church, 2017; Dai et al., 2023). Surface waters in this region are characterized by extremely low nutrient concentrations, limiting primary production (e.g., Dave and Lozier, 2010; Browning et al., 2021; Dai et al., 2023). Within the NPSG, the mean vertical advection acts as a sink for macronutrients, facilitated by basin-wide downwelling caused by Ekman convergence (Lee and Williams, 2000). In contrast, diapycnal fluxes of nutrients play a vital role in sustaining new/primary production by supplying nutrient-rich water from the deeper layers to the EZ (Kaneko et al., 2013; Fernández-Castro et al., 2015; Nagai et al., 2019; Tanaka et al., 2019; Kaneko et al., 2021; Mouriño-Carballido et al., 2021).

Studies on the western side of the North Pacific have shown an increasing trend in diffusive fluxes of nitrate with increasing vertical gradient of nitrate from oligotrophic subtropical gyre to non-oligotrophic subarctic waters (Kaneko et al., 2021). Diffusive fluxes of nitrate within the Kuroshio Current exhibit significant variability. Diffusive fluxes of nitrate on the northern Kuroshio axis are 1–2 orders of magnitude larger than those on the southern axis off the east coast of Japan due to enhanced mixing by active eddies and fronts (Kaneko et al., 2013; Nagai et al., 2019). Additionally, seamounts play an important role in enhancing diapycnal fluxes of nitrate. Tanaka et al. (2019) observed nitrate fluxes ranging from 10^{-2} to 10 mmol N m^{-2} d^{-1} across the Izu Ridge, which are 2–3 orders of magnitude larger than those in the open ocean and 1–2 orders of magnitude larger than those in the Kuroshio front.

Utilizing the relationship between the field determined diffusive fluxes of nitrate and environmental variables, Mouriño-Carballido et al. (2021) derived the diffusive fluxes of nitrate in the global ocean. Their study reported nitrate fluxes of 120 ± 10 μmol m^{-2} d^{-1} in the northwest subtropical Pacific, which are comparable to the sum of nitrogen fixation rates and atmospheric deposition. These results agreed with the finding of Fernández-Castro et al. (2015), who reported that diffusive fluxes of nitrate predominate over nitrogen fixation in the NPSG at the time of sampling. In contrast, based on measurements from 13 cruises conducted between 2014 and 2019, Hashihama et al. (2021) found that diffusive fluxes of nitrate are much lower than the sum of nitrogen fixation and atmospheric nitrogen deposition in the northwest NPSG. This finding is also supported by Yuan et al. (2023), who reported that the enhanced nitrogen fixation rather than diffusive fluxes of nitrogen, primarily drives the phosphate depletion in the upper NPSG. These discrepancies may stem from significant spatial and temporal variations in turbulent mixing and the relatively large uncertainties due to limited observational data. In addition, a limitation in prior estimates of nutrient flux is that most studies only consider nutrient flux induced by diapycnal diffusion, while diapycnal advection is often overlooked.

This study aims to investigate the diapycnal fluxes of nutrients and their ratios in the western NPSG, utilizing data from two cruises conducted during summer and winter. In addition to assessing diapycnal diffusive fluxes, we also consider the contribution of diapycnal advection in determining the diapycnal fluxes of nutrients. Furthermore, we explore factors influencing the spatial and seasonal variations in diapycnal fluxes of nutrients. Lastly, we apply a regression model in conjunction with a climatological nutrient dataset to examine the diapycnal fluxes of nutrients throughout the entire NPSG.

2. Data and methods

2.1. Sampling and measurements

Field observations were conducted in summer (July–August 2020) and winter (January–February 2021), on board the R/V TAN KAH KEE within the western NPSG (Fig. 1). The sampling region spanned from the Kuroshio (120.5°E) at west to the central NPSG (158°E) at east, and from the North Equatorial Current (NEC) at south at approximately 11°N to 33°N at north. A total of 18 and 11 stations were sampled during the summer and winter cruises, respectively.

Nutrient samples were collected at vertical intervals of approximately 10 m within the upper 200 m and approximately 50 m between 200 and 300 m. Samples were analyzed for NO_3^- + NO_2^- (NO_x^-) and dissolved inorganic phosphate (DIP) concentrations, including measurements at micro- and nanomolar levels. The nutrient analysis followed the methodology described by Du et al. (2017) and Yuan et al. (2023). Onboard analysis of nutrient concentrations at micromolar levels was performed using a Four-channel Continuous Flow Technicon AA3 Auto-Analyzer (Bran-Lube GmbH). The detection limits for NO_3^-, DIP, and NO_2^- were 0.1, 0.08 and 0.04 μmol L^{-1}, respectively. The analytical precision was 0.9 % for NO_3^-, 0.6 % for DIP and 10.4 % for NO_2^-. The determination of nanomolar levels of NO_x^- utilized a continuous flow analysis system combined with a liquid waveguide capillary flow cell, with a detection limit of 5.2 nmol L^{-1} and a precision of 4.7 % (Du et al., 2017; Yuan et al., 2023). DIP concentrations at the nanomolar level were determined using an onboard flow injection system, with a detection limit of 2.5 nmol L^{-1} and the precision was 11 %.

The discrete nutrient data were interpolated to have a one-meter vertical interval to match the high-resolution temperature and salinity data. Interpolation was performed using the relationship between

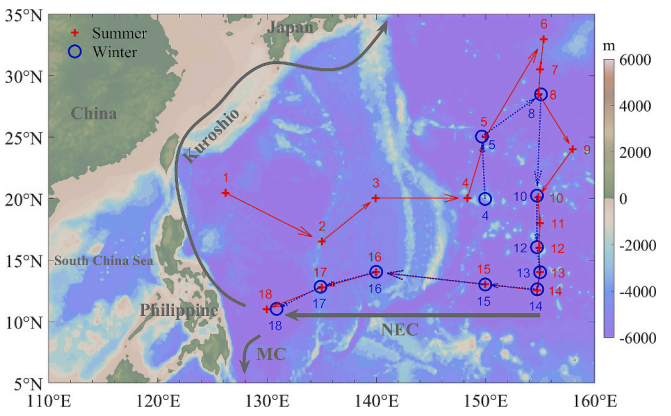

Fig. 1. Map of the western North Pacific Subtropical Gyre illustrating the bathymetry, sampling stations and the major ocean currents including the North Equatorial Current (NEC), Kuroshio Current, and Mindoro Current (MC). The red and blue arrows denote the cruise tracks in summer and winter, respectively. Note that some station names are the same between summer and winter but their locations are slightly different. (For interpretation of the references to colour in this figure legend, the reader is referred to the web version of this article.)

nutrients and potential density (σ_θ) due to their better alignment compared to the relationship between nutrients and depth in the ocean (Ascani et al., 2013; Omand and Mahadevan, 2013). The interpolation resulted in errors of less than 0.014 μmol L^{-1} and less than 0.051 μmol L^{-1} for NO_x^- concentrations below 0.1 μmol L^{-1} and above 0.1 μmol L^{-1}, respectively. For DIP concentrations, the interpolation errors were below 0.005 μmol L^{-1} and below 0.009 μmol L^{-1} for concentrations below 0.1 μmol L^{-1} and above 0.1 μmol L^{-1}, respectively. Since the distribution patterns of NO_x^- and DIP were similar, we primarily focus on NO_x^- unless stated otherwise in this paper.

Turbulence microstructures were measured using a VMP500 profiler (Rockland Scientific). The profiler was deployed in a free-fall way from the sea surface to a depth of approximately 500 m. The dissipation rate of turbulent kinetic energy (TKE) (ε) was determined by fitting the empirical Nasmyth spectrum to the measured shear spectra (Liu et al., 2017). Turbulence measurements were collected on 1 to 10 profiles at each station depending on sea conditions and ship time availability (see Table S1 for details). The station-averaged profiles of ε were used to calculate the diapycnal diffusivity. Thus, diffusivity estimates at stations with fewer sampling profiles are subject to larger uncertainties.

2.2. Methods for quantifying the diapycnal fluxes

The determination of diapycnal fluxes of nutrients follows the methods outlined by Du et al. (2017). Briefly, the diapycnal diffusivity K_v is calculated using the Osborn (1980) formula based on estimates of ε, i.e., $K_v = \varepsilon\Gamma/N^2$. Here, Γ is the mixing efficiency, and a canonical value of 0.2 is adopted (Gregg et al., 2018). N^2 denotes the squared buoyancy frequency, calculated as $N^2 = -g\rho_z/\rho_0$, with ρ_z representing the vertical gradient of the potential density, ρ_0 as a reference value for potential density, and g the acceleration due to gravity.

The diapycnal velocity w is calculated according to the formula derived firstly by McDougall (1984, 1987) based on neutral density surface analysis. The diapycnal fluxes of nutrients (F_v) are a summation of diapycnal diffusive flux ($F_{diff} = -K_v C_z$) and advective flux ($F_{adv} = wC$). Here, C_z denotes the vertical gradient of nutrient concentration (C), i.e., $\partial C/\partial z$. The C_z is calculated at every depth level using central-differential method. In addition, effective diapycnal flux (F_e) is defined as $F_e = F_{diff} + F_{adv} - F_H$, where F_H is the along-isopycnal divergence or convergence of C therein. F_e represents the net diapycnal influx of C to the water column between depth z and the sea surface. The equations, their derivations, and the accompanying explanations are detailed in the supplementary file of Du et al. (2017).

2.3. Calculating the background new production

The calculation of new/export production (NP) in this study follows the empirical equation proposed by Laws et al. (2011):

$$NP = NPP \times 0.04756\left(0.78 - \frac{0.43T}{30}\right)NPP^{0.307} \quad (1)$$

where, NPP represents the annual net primary productivity obtained from the Vertically Generalized Production Model available at http://sites.science.oregonstate.edu/ocean.productivity, while T corresponds to the annual mean sea surface temperature obtained from the World Ocean Atlas (WOA23) accessible at https://www.ncei.noaa.gov/access/world-ocean-atlas-2023.

3. Results

3.1. Hydrography and nutrient distributions

Located in the tropical and subtropical regions, the western NPSG exhibits noticeable variations in hydrography and NO_x^- concentrations. In summer, the conservative temperature (CT) in surface waters of the southwestern NPSG reached up to 30.7 °C, evidently higher than in the northern NPSG (Fig. 2a), with the lowest value down to 28.2 °C at Sta. 6. At depths of 50–150 m, the lowest CT values were found in the northern NPSG, while the highest values were mostly in the southern NPSG. Below 150 m, the pattern reversed, with the CT in the southern NPSG being evidently lower than in the other regions. If the North Pacific Subtropical Mode Water (STMW) was defined as having a CT between 16.0 and 19.0 °C (Oka, 2009), it was evident that the mode water in the northern NPSG ranged from 100 to over 300 m, much thicker than that in the other two regions, indicating that the northern NPSG was largely influenced by the STMW. In winter, in the upper 50 m, the CT was mostly lower than that in summer (Fig. 2b), with the lowest value of 22.8 °C observed in surface water at Sta. 8 in the northern NPSG.

In summer, in the upper 50 m, the absolute salinity (SA) in the northern and central NPSG was higher than in the southern part (Fig. 2c). At depths of 100–150 m, subsurface salinity maxima were clearly observed in the central and southern NPSG, whereas the northern NPSG exhibited weak or no subsurface salinity maxima. Below 200 m, the SA in the southern NPSG was generally lower than that in the other two regions. Seasonally, in the upper 50 m, the SA in summer was higher than in winter (Fig. 2c–d). At depth greater than 150 m, the seasonal changes in SA were not evident. The potential density anomaly (σ_θ) displayed an inverse distribution pattern compared to CT (Fig. 2e). In the upper 150 m, the σ_θ in the northern NPSG was significantly higher than in the central and southern NPSG. Below 150 m, the σ_θ in the southern NPSG was higher than in the other two regions. The σ_θ in winter display similar patterns to that in summer particularly at depths of >100 m (Fig. 2e–f).

There were significant differences in SA maximum at σ_θ of less than 24.8 kg m^{-3} (Fig. 3). In summer, the central NPSG was primarily characterized by a subsurface SA maximum with SA greater than 35.2 g kg^{-1} (Figs. 2c and 3a), indicative of the evident North Pacific Tropical Water (NPTW) (e.g., Qu et al., 1999). In contrast, the subsurface SA maximum in the southern NPSG was weak and thin. In the northern NPSG, the subsurface SA maximum was shallow, weak or even absent. The SA maximum in winter (Figs. 2d and 3b) exhibited an overall similar pattern to that in summer.

In summer, the squared buoyancy frequency, N^2, was below 0.1 × 10^{-4} s^{-2} within the surface mixed layer, and gradually increased to a maximum of approximately 6.0 × 10^{-4} s^{-2} at depths of 50 to 200 m, and then decreased to values below 1.0 × 10^{-4} s^{-2} at 300 m (Fig. 2g). Spatially, the N^2 maxima in the northern NPSG appeared at 10–50 m, which was much shallower than the 90–200 m range observed in the southern NPSG. At 100–300 m, the N^2 in the northern NPSG was significantly lower than that in the central and southern NPSG, suggesting low stratification attributed to the influence of STMW. As compared to summer, winter mostly displayed lower stratification in the upper 90 m (Fig. 2g–h), while below this depth, winter overall displayed higher stratification particularly in the central NPSG.

The NO_x^- concentrations exhibited an inverse distribution pattern relative to CT. In summer, NO_x^- concentrations were mostly below 0.1 μmol L^{-1}, characterizing a nutrient-depleted layer (NDL) within the upper 60–170 m, and increased to values ranging from 4.4 to 30.0 μmol L^{-1} at a depth of 300 m (Figs. 2i and 5d). In this study, the bottom of the NDL is defined as the depth where NO_x^- concentration reaches 0.1 μmol L^{-1} (Dai et al., 2023). It should be noted that this value serves as a practical definition, as the limited sampling resolution (~10 m) constrains our ability to precisely identify the top of the nutricline. This approach slightly overestimates the NDL depth and diapycnal fluxes. The NDL depth ranged from 56 to 116 m in the northern NPSG, evidently shallower than the 91–153 m range in the southern NPSG, and was significantly shallower than 108–170 m range in the central NPSG. From the bottom of the NDL to 200 m, NO_x^- concentrations in the central NPSG were lower than those in the northern and southern NPSG. Below 200 m, the southern NPSG exhibited the highest values compared to the other two regions. The seasonal variations of NO_x^- concentrations were not

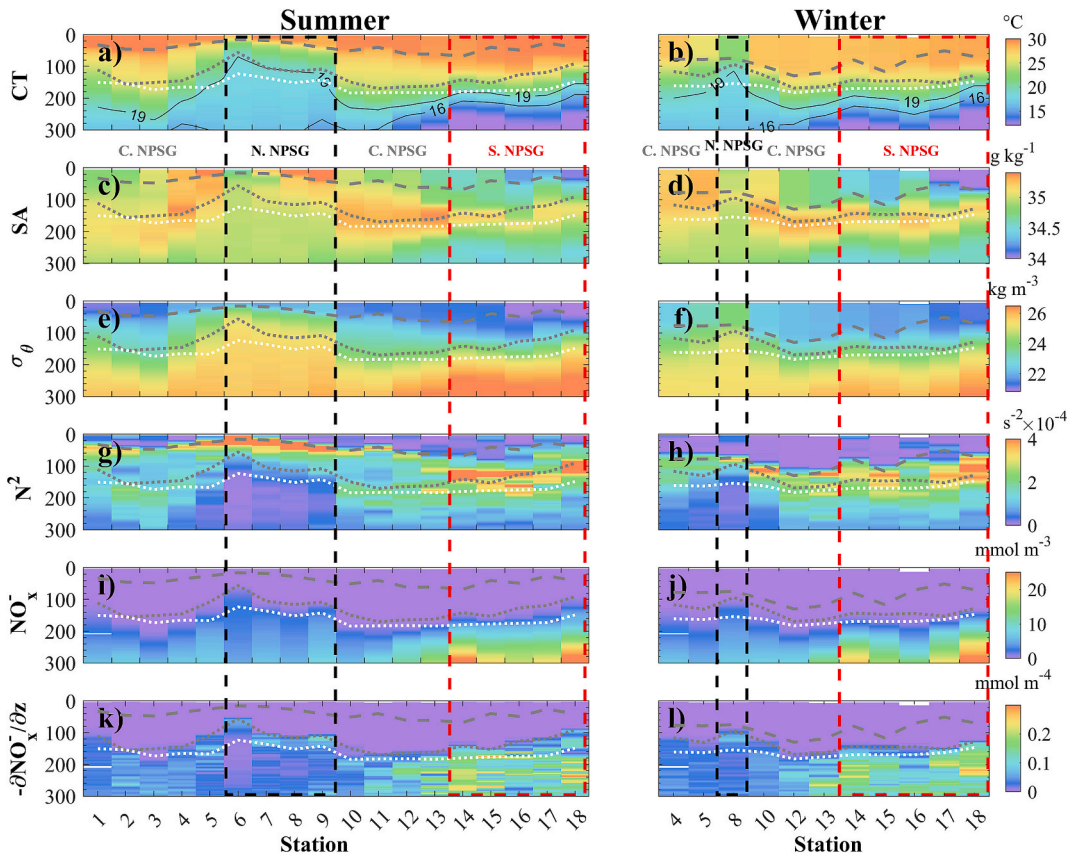

Fig. 2. Section distributions of the conservative temperature (CT, a–b), absolute salinity (SA, c–d), potential density anomaly (σ_θ, e–f), squared buoyancy frequency (N^2, g–h), concentrations of NO_3^- + NO_2^- (NO_x^-, i–j), and the negative vertical gradient of NO_x^- ($-\partial NO_x^-/\partial z$, k–l) within the upper 300 m of the North Pacific Subtropical Gyre (NPSG). The left column represents the summer season, and the right column represents the winter season. The gray dashed, gray dotted and white dotted lines denote the base of the mixed layer (defined as the depth at which σ_θ difference of 0.125 kg m^{-3} with respect to 10 m (Suga et al., 2004)), the nutrient-depleted layer (defined as the depth where NO_x^- concentration reaches 0.1 μmol L^{-1}) and euphotic zone, respectively. The stations located inside the black and red dashed lines are in the northern (N. NPSG, with a latitude range of roughly >24 °N) and southern (S. NPSG, with a latitude range of roughly <14 °N) NPSG, respectively. The stations located outside of the dashed rectangles illustrate the central NPSG (C. NPSG, with a latitude range roughly between 14 °N and 24 °N). The solid black contour lines in a) and b) denote the CT of 16.0 and 19.0 °C (Oka, 2009), which are used to quantify the boundaries of mode water in the NPSG. (For interpretation of the references to colour in this figure legend, the reader is referred to the web version of this article.)

evident (Fig. 2i-j).

In summer, the negative vertical gradients of NO_x^- ($-\partial NO_x^-/\partial z$) within the NDL were mostly close to 0.0 mmol m^{-4}, but increased to approximately 0.3 mmol m^{-4} within the 100–300 m depth range (Figs. 2k and 5e). Spatially, the central NPSG displayed noticeably lower $-\partial NO_x^-/\partial z$ values than the northern and southern NPSG. The highest $-\partial NO_x^-/\partial z$ values were observed at 150–200 m in the southern NPSG. The seasonal variations of $-\partial NO_x^-/\partial z$ were not evident (Fig. 2k–l).

Based on the spatial variations of CT, SA, σ_θ, water masses, and NO_x^- concentrations, we categorized our study area into three regions: (1) the southern NPSG, characterized by low sea surface salinity, high stratification at subsurface water and a shallower nutricline; (2) the northern NPSG, characterized by low sea surface temperature, weak stratification at subsurface water and a shallower nutricline, with subsurface influenced by STMW; (3) the central NPSG characterized by high sea surface salinity, a subsurface salinity maximum, and a deep nutricline evidently influenced by the NPTW.

3.2. Turbulence and diapycnal fluxes of nutrients

The TKE dissipation rate ε ranged $O(10^{-10}$–$10^{-5})$ W kg^{-1} in the upper 50 m and decreased to $O(10^{-10}$–$10^{-8})$ W kg^{-1} at 300 m (Figs. 4a–b and 5f). Spatially, at depths of <100 m, ε in the northern NPSG was generally lower than that in the southern and central NPSG. Seasonally, the averaged ε in winter was higher than in summer, particularly in the upper 200 m (Fig. 5f). Generally, the estimated ε values in this study were consistent with the microstructure measurements of Kaneko et al. (2021) but lower than $O(10^{-8})$ W kg^{-1} estimated by Whalen et al. (2018) using fine-scale parameterizations in the same region.

The diapycnal diffusivity K_V ranged from 10^{-7} to 10^{-5} m^2 s^{-1} at depth range of 70–300 m (Figs. 4c–d and 5g). The calculated K_V was consistent with field measurements of turbulence by Itoh et al. (2021) and Kaneko et al. (2021), suggesting relatively low K_V in the western NPSG. Although evident spatial heterogeneity of ε was observed, spatial variation of K_V was not apparent. This phenomenon can be attributed to the relationship between K_V, ε and N^2. In the northern NPSG, low ε and low N^2 tended to neutralize their effects on determining the values of K_V. By contrast, in the central and southern NPSG, K_V was primarily controlled by ε. Seasonally, the averaged K_V in winter was slightly larger than in summer particularly at depths <150 m and > 250 m. The diapycnal velocity w, with positive values indicating upward motions, ranged (−2.0 to 2.0) × 10^{-6} m s^{-1}, with mean values of (−0.5 to 2.0) × 10^{-7} m s^{-1} within the depth range of 100–300 m (Figs. 4e–f and 5h), predominantly showing an upward diapycnal motion.

Due to the small values of $-\partial NO_x^-/\partial z$, the diapycnal diffusive flux of NO_x^- (F_{diff_NOx}) in the NDL was mostly <1.0 μmol m^{-2} d^{-1} (Figs. 4g–h and 5i). These fluxes increased to maximum values of up to 121.1 μmol m^{-2} d^{-1} at depths of 150–250 m and then decreased to 3.9–21.5 μmol m^{-2} d^{-1} at 300 m. It should be noted that the formation of F_{diff_NOx}

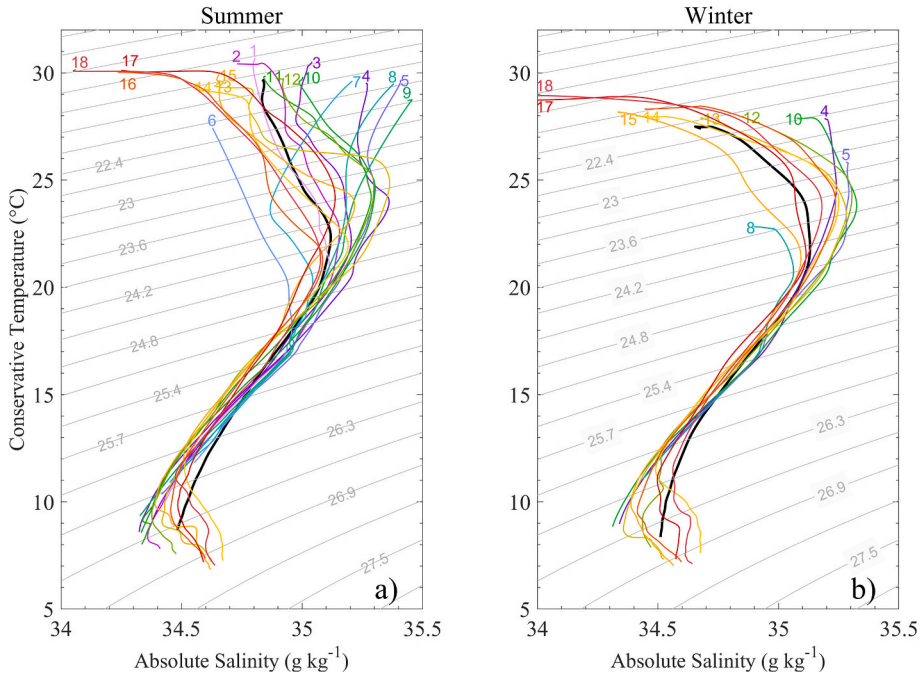

Fig. 3. The T-S diagrams in the upper 300 m of the western NPSG in summer and winter. The number labelled at the top of the plot denote the station illustrated in Figs. 1 and 2. The potential density anomaly (σ_θ) are superimposed on the T-S diagram.

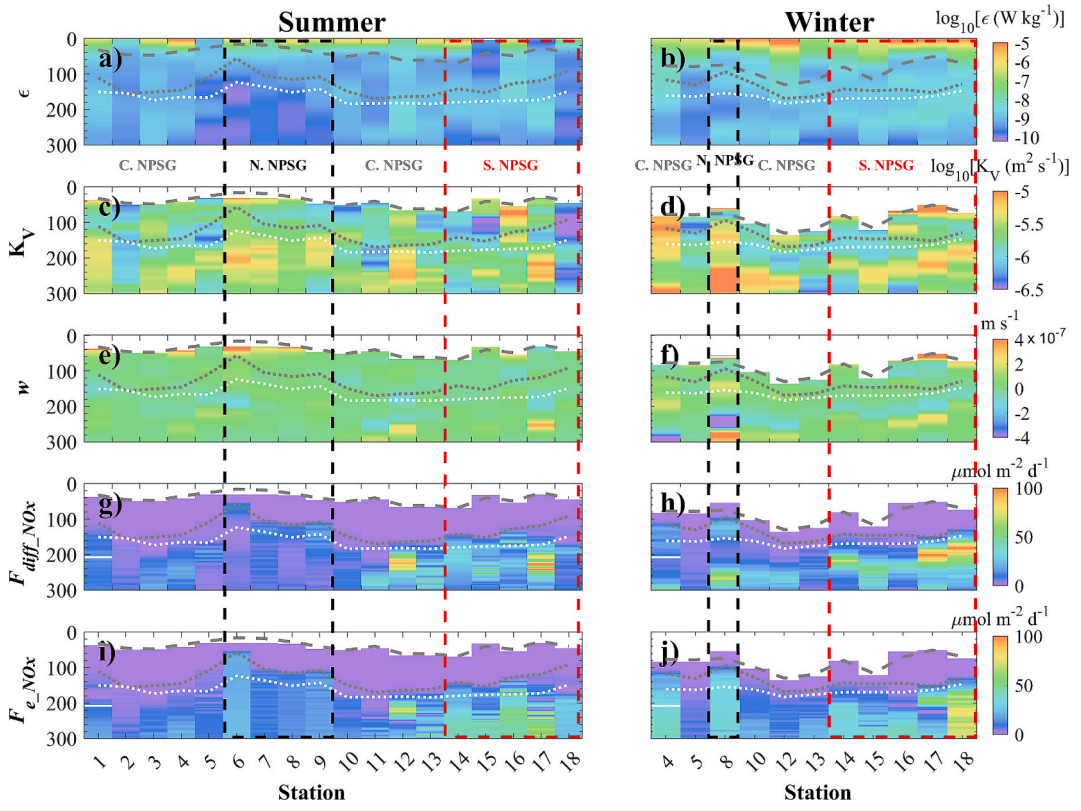

Fig. 4. Profiles of the TKE dissipation rate (ε, a–b), diapycnal diffusivity (K_V, c–d), diapycnal velocity (w, e–f), diapycnal diffusive flux of $NO_3^- + NO_2^-$ (NO_x^-) (F_{diff_NOx}, g–h), and effective diapycnal flux of NO_x^- (F_{e_NOx}, i–j). The stations located inside the black and red dashed lines are in the northern (N. NPSG) and southern (S. NPSG) NPSG, respectively. Conversely, the stations located outside of the rectangles denote the central NPSG stations (C. NPSG). (For interpretation of the references to colour in this figure legend, the reader is referred to the web version of this article.)

maxima at these depths is controlled by complex physical and biological processes. Briefly, the F_{diff_NOx} is a product of K_V and $-\partial NO_x^-/\partial z$, where K_V is governed by turbulence intensity and density stratification, and $-\partial NO_x^-/\partial z$ maxima result from various biogeochemical processes, including vertical variability in biological consumption, remineralization, as well as both diapycnal and isopycnal transports. These processes

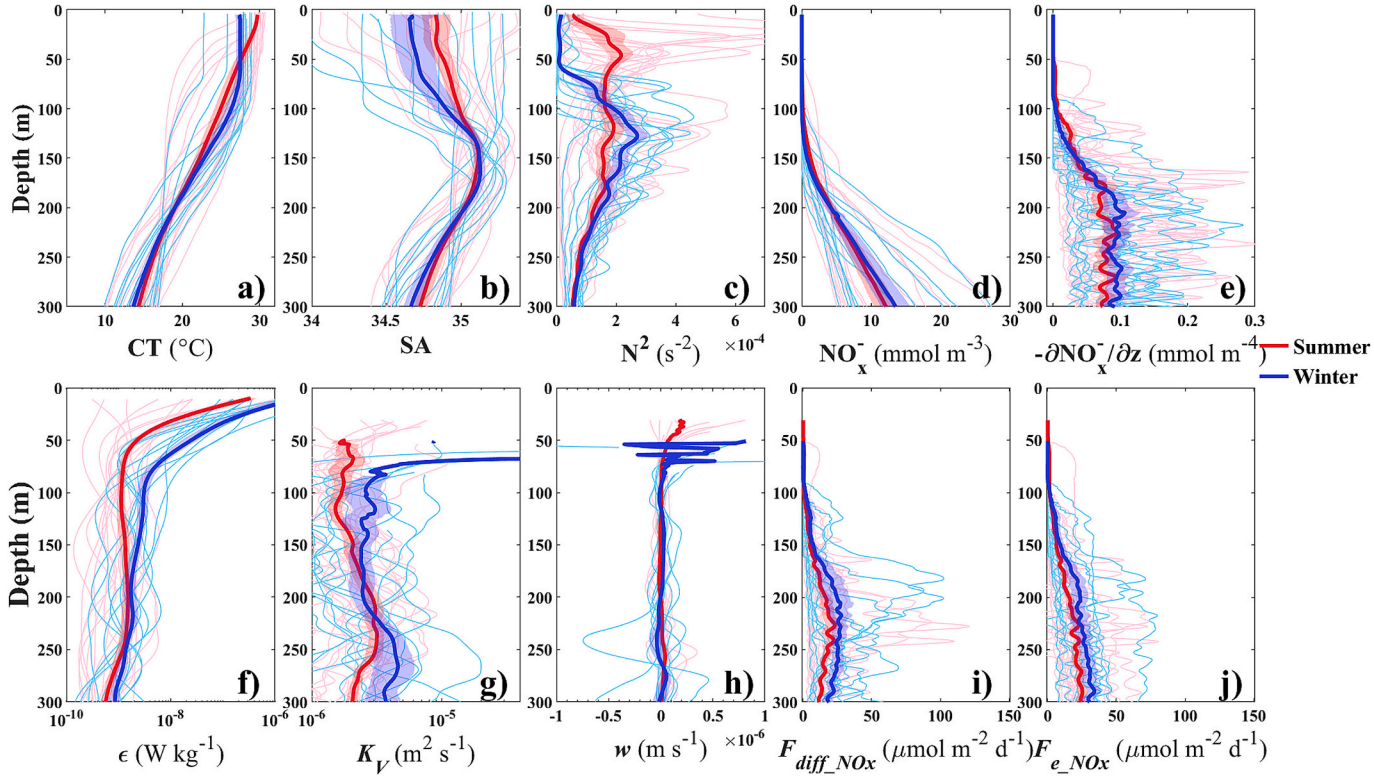

Fig. 5. Depth profiles of the conservative temperature (CT, a), absolute salinity (SA, b), squared buoyancy frequency (N^2, c), NO_3^- + NO_2^- (NO_x^-, d) concentrations, NO_x^- gradient ($-\partial NO_x^-/\partial z$, e), TKE dissipation rate (ϵ, f), diapycnal diffusivity (K_V, g), diapycnal velocity (w, b), diapycnal diffusive flux of NO_x^- (F_{diff_NOx}, i), and effective diapycnal flux of NO_x^- (F_{e_NOx}, j) in summer and winter, respectively. The thick lines represent the cruise mean values, while the shaded areas indicate the standard deviations of the cruise mean obtained through bootstrap sampling.

jointly determined the depth of F_{diff_NOx} maxima, which should be carefully investigated in the future.

Spatially, in the upper 100 m, F_{diff_NOx} in the northern NPSG exhibited higher values than the central and southern NPSG. Conversely, below 150 m, the southern NPSG displayed higher values of F_{diff_NOx} than the other two regions. Seasonally, at the same depth, the averaged F_{diff_NOx} in winter was higher than that in summer. The effective diapycnal flux of NO_x^-, F_{e_NOx}, which reflects the net influx of diapycnal flux of NO_x^- towards the upper water column, resembled the F_{diff_NOx} and was mostly <1.0 μmol m^{-2} d^{-1} in the NDL (Figs. 4i–j and 5j). These fluxes

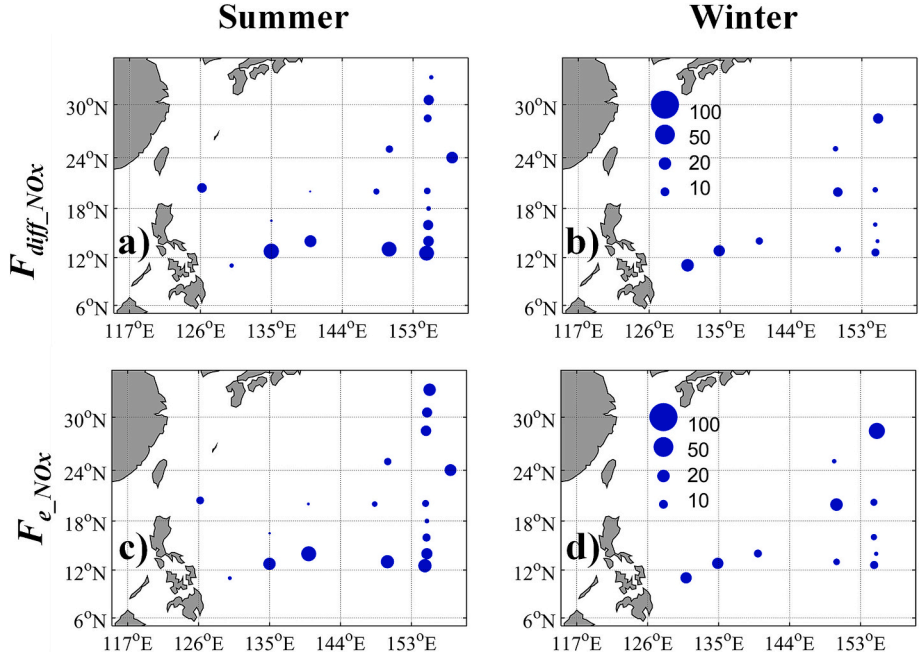

Fig. 6. Spatial and seasonal variations of the diapycnal diffusive flux (F_{diff_NOx}, a–b, in μmol m^{-2} d^{-1}) and effective diapycnal flux (F_{e_NOx}, c–d, in μmol m^{-2} d^{-1}) of NO_x^- in summer and winter seasons.

increased to up to 80.7 μmol m^{-2} d^{-1} at depths of 200–300 m. The averaged F_{e_NOx} in winter was slightly higher than that in summer.

3.3. Diapycnal fluxes of nutrients to the euphotic zone

The euphotic zone, EZ, was defined as the depth where 0.1 % of the surface photosynthetic active radiation is available. In this section, we pay particular attention to the nutrient fluxes to the EZ. The cruise mean values for EZ depth were 162 ± 19 m and 163 ± 10 m in summer and winter, respectively (Fig. 6a–d). Note that this seasonal pattern contradicts with the findings of Letelier et al. (2004), who reported significantly higher EZ in summer than in winter at Sta. ALOHA. The discrepancy might be attributed to the following factors: (1) the seasonal variations of EZ are small in the western NPSG (Dai et al., 2023); (2) the lack of overlapping sampling stations between summer and winter, particularly in the northern NPSG; (3) the fact that these averages fall within the range of standard deviation errors. Note also that we focus on NO_x^- fluxes at the base of the EZ, rather than at the depths of F_{diff_NOx} and $-\partial NO_x^-/\partial z$ maxima, because F_{diff_NOx} at the base of the EZ represents the supply of new nutrients and corresponds to new production to the EZ. Additionally, the EZ depths are consistently deeper than the NDL (Fig. 4g–j), suggesting that the base of the EZ located within the nitracline.

At the base of the EZ, the F_{diff_NOx} ranged 0.6 to 30.2 μmol m^{-2} d^{-1}. Higher values were mostly found in the southern and northern NPSG. Seasonally, the cruise averaged F_{diff_NOx} was 11.7 ± 9.6 and 8.5 ± 6.1 μmol m^{-2} d^{-1} in summer and winter, respectively. Our estimations are larger than <0.8 μmol m^{-2} d^{-1} estimated by Kaneko et al. (2021) in this region, but are comparable to the values of 10.7 ± 2.6 μmol m^{-2} d^{-1} estimated by Hashihama et al. (2021) along a 24°N zonal transect (133.0–140.3°E). The cruise averaged F_{e_NOx} was 11.9 ± 8.6 and 11.3 ± 9.3 μmol m^{-2} d^{-1} in summer and winter, respectively. F_{e_NOx} displayed similar or slightly larger values than F_{diff_NOx}, suggesting that F_{e_NOx} was primarily determined by F_{diff_NOx}. Thus, the diapycnal advection plays a secondary role on NO_x^- transport in the EZ, which is consistent with previous studies (Du et al., 2017).

The spatial and seasonal patterns of the diapycnal diffusive flux (F_{diff_DIP}) and effective diapycnal flux (F_{e_DIP}) of DIP closely resembled those of NO_x^- (Figs. S1 and S2). At the base of the EZ, the cruise-averaged F_{diff_DIP} (F_{e_DIP}) values were 0.64 ± 0.58 (0.61 ± 0.65) and 0.66 ± 0.49 (0.85 ± 0.73) μmol m^{-2} d^{-1} in summer and winter, respectively. The ratios of F_{diff_NOx} to F_{diff_DIP} were 18.2 ± 2.0 and 13.9 ± 2.0 in summer and winter, respectively. These flux ratios exceeded or approximated the canonical Redfield ratio of 16:1 and were significantly higher than the concentration ratios of 10.4 ± 1.1, and 7.4 ± 1.2 at the base of the EZ in summer and winter, respectively (Fig. S3). According to the definitions, the diffusive flux ratio is determined by the concentration gradient rather than the concentration itself, making it fundamentally different from the concentration ratio. Therefore, as compared to the concentration ratio, a larger $F_{diff\_NOx}/F_{diff\_DIP}$ ratio suggests a relatively steeper nitracline than phosphacline (P-nutricline). This phenomenon warrants further investigations in relation to non-Redfield nutrient consumption, N_2-fixation, and the decoupling of remineralization between nitrogen and phosphorus. Future studies should place greater emphasis on nutrient gradient ratios rather than concentration ratios. In addition, the elevated N:P flux ratio can supply relatively more excess nitrogen, implying that nitrogen limitation could be relieved by diapycnal transports.

4. Discussion

4.1. Factors influencing the diapycnal fluxes

In order to investigate the factors driving the spatial and seasonal variations of diapycnal fluxes at the base of the EZ, we performed correlation analyses between the factors of Q, $1/N^2$, and $-\partial NO_x^-/\partial z$ with F_{diff_NOx} and F_{e_NOx}. The use of $1/N^2$ instead of N^2 allowed for a straightforward analysis of the factors influencing K_V, given that $K_V = \Gamma\varepsilon/N^2$. Linear regression models were employed for the logarithmic correlation analysis. As the correlations in summer and winter are similar, we integrate the summer and winter data together to examine the correlations to reduce the regression error (Fig. 7). The logarithm of F_{diff_NOx} exhibited a strong linear relationship with the logarithm of $-\partial NO_x^-/\partial z$ (slope = 1.16, $R^2 = 0.63$, $p < 0.01$; Fig. 7c), suggesting that $-\partial NO_x^-/\partial z$ are the main factors influencing the spatial and seasonal variations of F_{diff_NOx}. Additionally, the correlation between the logarithm of F_{diff_NOx} and ε (slope = 1.36, $R^2 = 0.26$, $p < 0.01$; Fig. 7a) displayed weak and positive correlations. Conversely, the correlation between the logarithm of F_{diff_NOx} and logarithm of $1/N^2$ was found to be insignificant ($R^2 = 0.01$, $p = 0.66$; Fig. 7b). Similar patterns were observed for F_{e_NOx}, with correlation coefficients being lower than those for F_{diff_NOx} (Fig. 7d–f). These results suggest that $-\partial NO_x^-/\partial z$ plays a more important role than ε and $1/N^2$ on spatial variations of F_{diff_NOx} and F_{e_NOx}. This implies that apart from examining changes due to global warming on stratification and nutrient concentrations (e.g., Gruber, 2011; Cabré et al., 2015; Fu et al., 2016; Nakamura and Oka, 2019), changes to vertical nutrient gradients should also be taken into account. Similar patterns have also been observed for DIP (Fig. S4).

4.2. Diapycnal fluxes of nutrients in the NPSG

As discussed in Section 4.1, a strong linear relationship was observed between the decimal logarithm of $-\partial NO_x^-/\partial z$ and F_{diff_NOx} (F_{e_NOx}) at the base of the EZ in the NPSG. Building upon this linear regression model and utilizing nutrient data obtained from the WOA23, we further predicted F_{diff_NOx} and F_{e_NOx} across the entire NPSG on a climatological annual scale (Fig. 8a–b).

The predicted F_{diff_NOx} and F_{e_NOx} exhibit similar patterns and range from 1 to 100 μmol m^{-2} d^{-1} within the NPSG (Fig. 8a–b). In the central and western NPSG, F_{diff_NOx} and F_{e_NOx} range from 1 to 10 μmol m^{-2} d^{-1}, notably lower than the values ranging from 10 to 100 μmol m^{-2} d^{-1} in the southern and eastern NPSG. The spatial pattern of F_{diff_NOx} aligns with previous studies conducted by Mouriño-Carballido et al. (2021). However, our values were approximately one order of magnitude lower, particularly in the central and western NPSG. The limited spatial coverage of observational data in Mouriño-Carballido et al. (2021), particularly in the central and western Pacific, may introduce substantial uncertainties in their flux estimates, potentially explaining the discrepancies between our results and theirs in this region. Overall, the spatially averaged F_{diff_NOx} (F_{e_NOx}) and F_{diff_DIP} (F_{e_DIP}) are 18.3 ± 15.5 (20.2 ± 16.6) and 1.1 ± 0.8 (1.5 ± 1.3) μmol m^{-2} d^{-1} in the entire NPSG, respectively.

The new production NP was calculated using an empirical equation proposed by Laws et al. (2011) (see Section 2.3 for details), which was converted to nitrogen (NP_N) using a carbon to nitrogen ratio of 6.96:1 (Martiny et al., 2013). In the NPSG, the NP_N is 117–1310 μmol m^{-2} d^{-1} with low values found in the western and central NPSG (Fig. 8c). We define the F_{e_NOx}/NP_N to show the contributions of diapycnal fluxes to the NP_N. In the southern NPSG close to the NEC, the F_{e_NOx}/NP_N is >0.2 (Fig. 8d). By contrast, the F_{e_NOx}/NP_N is mostly <0.05 in the rest of NPSG, suggesting that diapycnal flux of NO_x^- plays a minor role, and other nitrogen sources such as N_2-fixation and lateral transport might play important roles on nitrogen budget (Letscher et al., 2016). The averaged F_{e_NOx}/NP_N in the entire NPSG is 8.5 ± 8.3 %, respectively. This proportion is lower than 13–32 % between 40°N and 40°S estimated by Mouriño-Carballido et al. (2021). If we use a carbon to phosphorus ratio of 195:1 (Martiny et al., 2013), the ratio of F_{e_DIP} to phosphorus required by new production (NP_P, F_{e_DIP} / NP_P) is 18.1 ± 17.9 % (Fig. S5), which is more than twice as large as than that for nitrogen. This suggests that the diapycnal fluxes play a more important role on the DIP budget and highlights the decoupling of nitrogen and

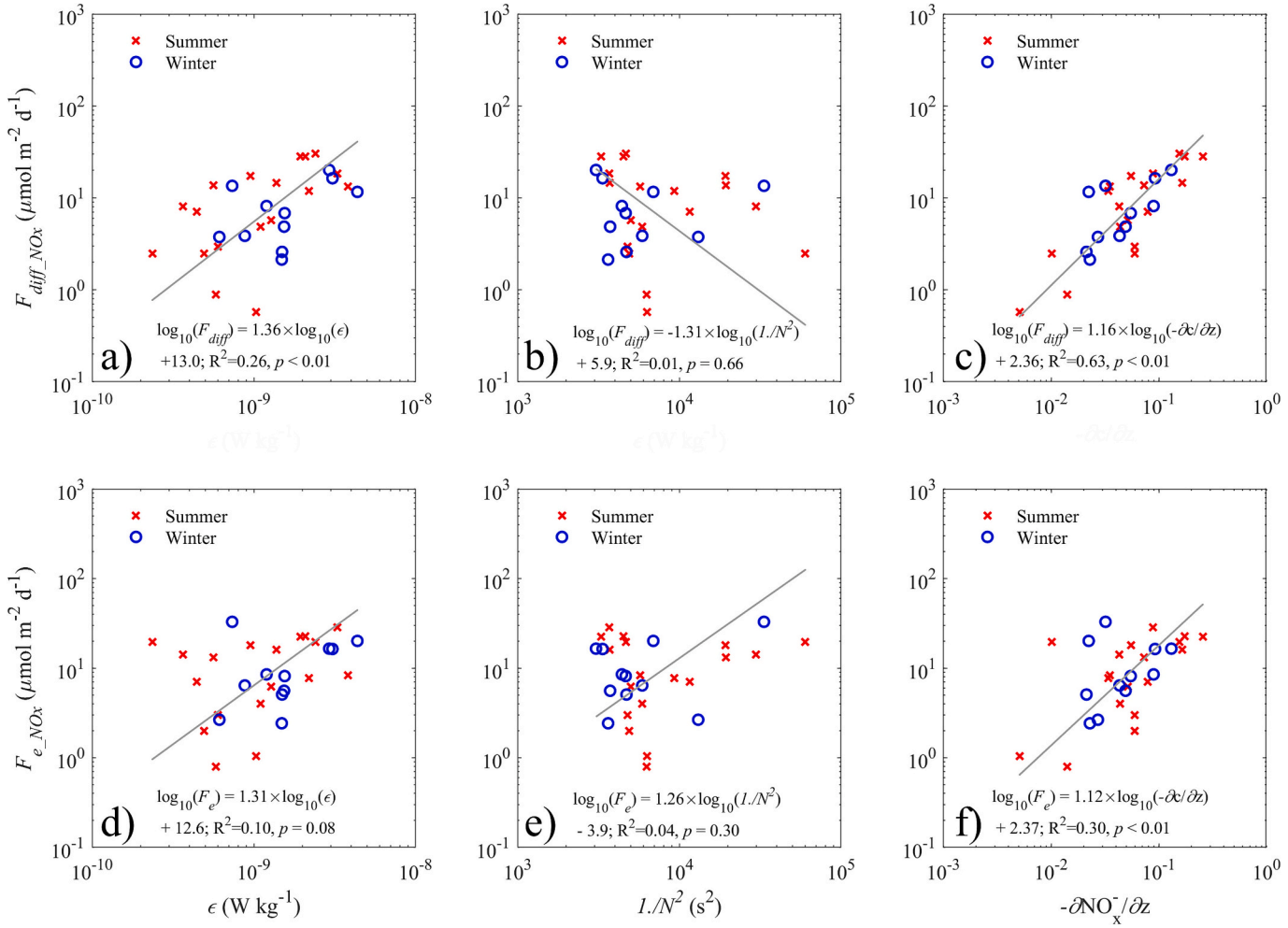

Fig. 7. Correlation analysis between diapycnal diffusive flux (F_{diff_NOx}) and effective diapycnal flux (F_{e_NOx}) of NO_x^-, along with the parameters ε (a, d), $1/N^2$ (b, e) and $-\partial NO_x^-/\partial z$ (c, f). The texts and number denote the regression equation, coefficient of determination (R^2) and the p value. Noted that the regression analysis is performed using logarithmic relationships between the fluxes and the parameters.

phosphorus cycles in the upper oligotrophic ocean.

The integrated N_2-fixation rate ranges from 10 to 1000 μmol m^{-2} d^{-1} in the NPSG (Dai et al., 2023 and references therein) with higher values found in the central NPSG. Spatially, the F_{diff_NOx} exhibited an inverse pattern to N_2-fixation rate, supporting the precedent that high NO_x^- fluxes could reduce the N_2-fixation potential. Additionally, the N_2-fixation rate determined during the same cruises were 252.4 ± 221.4 and 75.1 ± 78.7 μmol m^{-2} d^{-1} in summer and winter, respectively (Yu et al., 2024). These values were 7–20 times larger than F_{diff_NOx} and F_{e_NOx}, suggesting that N_2-fixation dominated over diapycnal fluxes of NO_x^-.

Limited observations found that the total dry deposition of reactive nitrogen ranged 5.0–1100 μmol m^{-2} d^{-1}, mostly on the order of 10.0–100.0 μmol m^{-2} d^{-1} (Martino et al., 2014; Qi et al., 2020; Dai et al., 2023 and reference therein). Based on five cruise observations, Hashihama et al. (2021) estimated that the total atmospheric nitrogen deposition, including organic nitrogen, was 27.4 ± 3.3 μmol m^{-2} d^{-1}. Similarly, based on four cruises conducted in the NPSG, Qi et al. (2020) estimated that the atmospheric inorganic nitrogen deposition rate was 22.3 ± 12.1 μmol m^{-2} d^{-1}. All these values are evidently larger than the F_{diff_NOx} and F_{e_NOx}, suggesting once again that the diapycnal NO_x^- fluxes play a minor role on nitrogen budget in the oligotrophic NPSG. In contrast, the atmospheric phosphate deposition ranges 0.04–0.08 μmol m^{-2} d^{-1} (Martino et al., 2014; Qi et al., 2020). Diapycnal flux of phosphate was roughly ten times larger than the atmospheric phosphorus deposition. These results further indicate a decoupling of nitrogen and phosphorous cycling in the upper ocean. It should be noted that these estimates represent spatially averaged values. Additionally, the atmospheric nitrogen deposition in the western and northern NPSG is larger than that in other regions of the NPSG (e.g., Duce et al., 2008; Luo et al., 2018; Hamilton et al., 2022). This pattern contrasts with F_{diff_NOx} and F_{e_NOx}, implying the diapycnal transport may play relatively more important role in the eastern NPSG than in the western region. Furthermore, current levels of anthropogenic nitrogen deposition exceed pre-industrial levels (Duce et al., 2008), implying the anthropogenic nitrogen deposition now plays a more and more important role in the current ocean. However, it should be noted that diapycnal fluxes, N_2-fixation, and atmospheric deposition all contribute to additional nitrogen relative to phosphorus input (deviating from the canonical Redfield ratio) and can relive nitrogen limitation in the upper NPSG.

In this study, we applied an average C:N ratio of 6.96:1 for the warm, nutrient-depleted subtropical gyre, following Martiny et al. (2013). However, other studies, have reported varying values. For example, Geider and La Roche (2002) reported a mean C:N ratio of 7.3 in marine particulate matter, with a 95 % confidence range of 6.8–7.8. Karl and Church (2017) reported an average particulate C:N flux ratio of 8.0 at 150 m depth at the Hawaii Ocean Time-series (HOT) station. Additionally, using global particulate organic matter data, Tanioka et al. (2022) reported an average C:N ratio of 6.7 in the subtropical ocean. Based on these values, a range of C:N ratios from 6.7 to 8.0 could introduce a maximum error of 14.9 % for NP_N when compared to a fixed

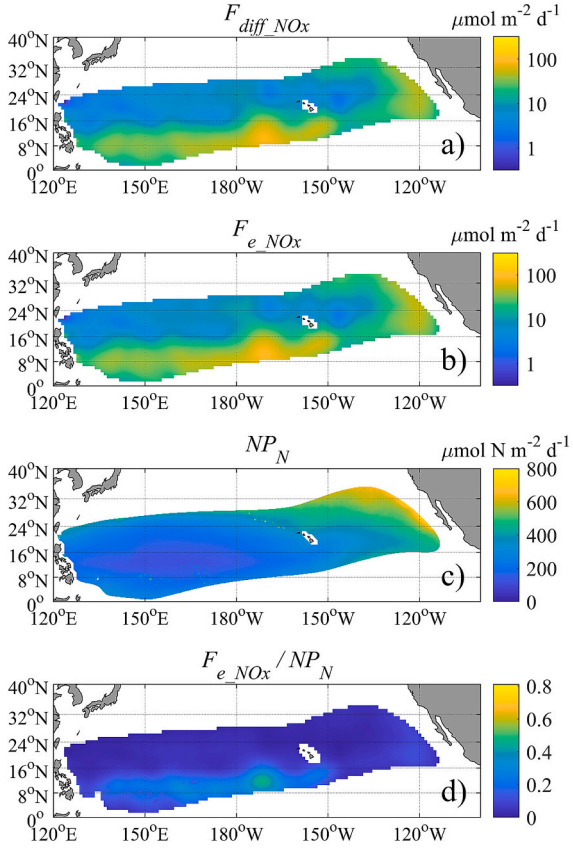

Fig. 8. Distributions of the diapycnal diffusive flux (F_{diff_NOx}) (a) and effective diapycnal flux (F_{e_NOx}) (b) of NO_x^- obtained from the linear regression models described in Section 4.2; new production required nitrogen (NP_N) (c); F_{e_NOx} to NP_N ratio (d). It should be noted that these results represent annual mean values (see main text for methodological details).

C:N ratio of 6.96:1. Similarly, an average C:P ratio of 195:1 was applied according to Martiny et al. (2013). This selection could introduce a maximum error of 41.5 % for NP_P when applying a C:P ratio ranging from 114:1 to 195:1, as reported in various studies (Geider and La Roche, 2002; Martiny et al., 2013; Tanioka et al., 2022).

Seamounts have been found to be able to enhance turbulent mixing and subsequently increase the diapycnal fluxes of nutrients in oligotrophic oceans (Tanaka et al., 2019; Tuerena et al., 2019). However, most of our sampling stations are located far from seamount areas (Fig. 1). Therefore, the diapycnal fluxes of nutrients estimated in this study may underestimate the total diapycnal fluxes in the NPSG. Furthermore, the spatial distribution of nutrient fluxes is influenced by the number of turbulence measurements conducted at each station; stations with more turbulence profiles are subject to greater confidence in flux estimates. Finally, since our sampling locations are concentrated in the western NPSG, estimates for the eastern NPSG may contain additional errors that were not evaluated in this study.

5. Concluding remarks

Based on two-cruise measurements conducted in summer and winter, we have revealed the spatial and seasonal variations in hydrography, nutrient, and diapycnal fluxes of nutrients in the western NPSG. The hydrography analyses revealed that the southern NPSG was evidently influenced by NEC, central NPSG evidently influenced by NPTW, and the northern NPSG evidently influenced by North Pacific STMW. The TKE dissipation rate ε ranged $O(10^{-10}$–$10^{-8})$ W kg^{-1} between 50 and 300 m, and displayed lowest values in the northern NPSG. The diapycnal diffusivity K_V ranged $O(10^{-7}$–$10^{-5})$ m^2 s^{-1} at depths of 70–300 m. Both F_{diff_NOx} and F_{e_NOx} showed minimal values in the NDL and increased with depth in the upper 250 m. In the upper 250 m, F_{e_NOx} was primarily determined by F_{diff_NOx}. Spatially, higher values were found in the southern NPSG influenced by the NEC and in the northern NPSG influenced by the North Pacific STMW. At the base of the EZ, the cruise averaged F_{diff_NOx} (F_{e_NOx}) was 11.7 ± 9.6 (11.9 ± 8.6) and 8.5 ± 6.1 (11.3 ± 9.3) μmol m^{-2} d^{-1} in summer and winter, respectively. Seasonal variations are not evident.

The cruise averaged flux ratio of F_{diff_NOx} to F_{diff_DIP} was 18.2 ± 2.0 and 13.9 ± 2.0, significantly higher than the NO_x^-:DIP concentration ratio of 10.4 ± 1.1 and 7.4 ± 1.2 observed at the base of the EZ in summer and winter, respectively. As compared to a lower N:P concentration ratio implying nitrogen limitation in the upper water column, the elevated diapycnal flux ratio of N:P could transport more excess NO_x^-, and potentially relieve the nitrogen limitation in the upper NPSG.

Spatial variations in diapycnal fluxes of nutrients were primarily controlled by the vertical gradient of nutrients instead of ε and stratifications, suggesting that the former is the key factors to influence the diapycnal fluxes of nutrients. This phenomenon is further employed to predict diapycnal fluxes of nutrients in the entire NPSG. The predicted F_{diff_NOx} and F_{e_NOx} range from 1 to 10 μmol m^{-2} d^{-1} in the central and western NPSG, which are lower than 10–100 μmol m^{-2} d^{-1} in the southern and eastern NPSG. The spatially averaged F_{diff_NOx} (F_{e_NOx}) is estimated to be 18.3 ± 15.5 (20.2 ± 16.6) μmol m^{-2} d^{-1}, contributing approximately 8.1 ± 8.2 % (8.5 ± 8.3 %) of the new production in the entire NPSG. Spatially, the higher F_{diff_NOx} (F_{e_NOx}) correspond to low N_2-fixaiton. The averaged F_{diff_NOx} and F_{e_NOx} were much lower than fluxes of N_2-fixation or atmospheric nitrogen deposition, playing a minor role on nitrogen budget in the upper NPSG. In contrast, F_{e_DIP} contributes to 18.1 ± 17.9 % of the NP_P, and is roughly ten times larger than the atmospheric phosphorus deposition.

CRediT authorship contribution statement

Chuanjun Du: Writing – review & editing, Visualization, Investigation, Formal analysis, Writing – original draft, Methodology, Funding acquisition, Conceptualization. **Minhan Dai:** Writing – original draft, Funding acquisition, Writing – review & editing, Supervision, Conceptualization. **Zhiyu Liu:** Writing – review & editing, Resources, Conceptualization, Writing – original draft, Methodology. **Zhendong Hu:** Methodology, Writing – review & editing, Investigation. **Jin-Yu Terence Yang:** Writing – review & editing, Investigation, Writing – original draft. **Kuanbo Zhou:** Methodology, Writing – review & editing, Investigation. **Hongyang Lin:** Writing – review & editing, Investigation, Methodology. **Zhongwei Yuan:** Methodology, Writing – review & editing, Investigation. **Lifang Wang:** Writing – review & editing, Investigation, Methodology. **Tao Huang:** Methodology, Writing – review & editing, Investigation. **Liguo Guo:** Writing – review & editing, Investigation, Methodology. **Zhe Wang:** Methodology, Writing – review & editing, Investigation. **Shuh-Ji Kao:** Writing – review & editing, Conceptualization, Investigation.

Declaration of generative AI and AI-assisted technologies in the writing process

During the preparation of this work, the ChatGPT was solely and lightly used to improve readability and language prior to submission. After using this tool, the authors reviewed and edited the content as needed and take full responsibility for the content of the publication.

Declaration of competing interest

The authors declare that they have no known competing financial interests or personal relationships that could have appeared to influence the work reported in this paper.

Acknowledgements

This study was funded by the National Key Research and Development Program of China (2023YFF0805001), Strategic Priority Research Program of the Chinese Academy of Sciences (XDB42000000), Innovational Fund for Scientific and Technological Personnel of Hainan Province (KJRC2023B04), National Natural Science Foundation of China (42494885, 42492881, 42188102, 41890801), Research Grants Council of the Hong Kong Special Administrative Region, China (AoE/P-601/23-N), and Provincial Natural Science Foundation of Hainan (624MS037). We are grateful to the captain and crew of R/V *TAN KAH KEE* for their assistance in the sampling and/or data analysis during the cruise. Zhimian Cao is thanked for providing useful information. Fangtao Zhang and Zhiyong Cao are thanked for conducting microstructure measurements.

Appendix A. Supplementary data

Supplementary data to this article can be found online at https://doi.org/10.1016/j.gloplacha.2025.104973.

Data availability

Data will be made available on request.

References

Arrigo, K.R., 2005. Marine microorganisms and global nutrient cycles. Nature 437, 349–355.

Ascani, F., Richards, K.J., Firing, E., Grant, S., Johnson, K.S., Jia, Y., Lukas, R., Karl, D. M., 2013. Physical and biological controls of nitrate concentrations in the upper subtropical North Pacific Ocean. Deep-Sea Res. II 93, 119–134.

Browning, T.J., Moore, C.M., 2023. Global analysis of ocean phytoplankton nutrient limitation reveals high prevalence of co-limitation. Nat. Commun. 14 (1), 5014. https://doi.org/10.1038/s41467-023-40774-0.

Browning, T.J., Liu, X., Zhang, R., Wen, Z., Liu, J., Zhou, Y., Xu, F., Cai, Y., Zhou, K., Cao, Z., Zhu, Y., Shi, D., Achterberg, E.P., Dai, M., 2021. Nutrient co-limitation in the subtropical Northwest Pacific. Limnol. Oceanogr. Lett. 7 (1), 52–61.

Cabré, A., Marinov, I., Leung, S., 2015. Consistent global responses of marine ecosystems to future climate change across the IPCC AR5 earth system models. Climate Dynam. 45 (5–6), 1253–1280.

Dai, M., Luo, Y., Achterberg, E.P., Browning, T.J., Cai, Y., Cao, Z., Chai, F., Chen, B., Church, M.J., Ci, D., Du, C., Gao, K., Guo, X., Hu, Z., Kao, S., Laws, E.A., Lee, Z., Lin, H., Liu, Q., et al., 2023. Upper Ocean biogeochemistry of the oligotrophic North Pacific subtropical gyre: from nutrient sources to carbon export. Rev. Geophys. 61 (3), e2022RG000800. https://doi.org/10.1029/2022rg000800.

Dave, A.C., Lozier, M.S., 2010. Local stratification control of marine productivity in the subtropical North Pacific. J. Geophys. Res. 115 (C12), C12032. https://doi.org/10.1029/2010jc006507.

Du, C., Liu, Z., Kao, S., Dai, M., 2017. Diapycnal fluxes of nutrients in an oligotrophic oceanic regime: the South China Sea. Geophys. Res. Lett. 44 (22), 11510–11518.

Duce, R.A., LaRoche, J., Altieri, K., Arrigo, K.R., Baker, A.R., et al., 2008. Impacts of atmospheric anthropogenic nitrogen on the open ocean. Science 320 (5878), 893–897.

Fernández-Castro, B., Mouriño-Carballido, B., Marañón, E., Chouciño, P., Gago, J., Ramírez, T., Vidal, M., Bode, A., Blasco, D., Royer, S., Estrada, M., Simó, R., 2015. Importance of salt fingering for new nitrogen supply in the oligotrophic ocean. Nat. Commun. 6 (1), 8002. https://doi.org/10.1038/ncomms9002.

Fu, W., Randerson, J.T., Moore, J.K., 2016. Climate change impacts on net primary production (NPP) and export production (EP) regulated by increasing stratification and phytoplankton community structure in the CMIP5 models. Biogeosciences 13 (18), 5151–5170. https://doi.org/10.5194/bg-13-5151-2016.

Geider, R., La Roche, J., 2002. Redfield revisited: variability of C:N:P in marine microalgae and its biochemical basis. Eur. J. Phycol. 37 (1), 1–17. https://doi.org/10.1017/s0967026201003456.

Gregg, M., D'Asaro, E., Riley, J., Kunze, E., 2018. Mixing efficiency in the ocean. Ann. Rev. Mar. Sci. 10 (1), 443–473.

Gruber, N., 2011. Warming up, turning sour, losing breath: ocean biogeochemistry under global change. Philos. Trans. R. Soc. A 369 (1943), 1980–1996.

Hamilton, D.S., Perron, M.M.G., Bond, T.C., Bowie, A.R., Buchholz, R.R., Guieu, C., et al., 2022. Earth, wind, fire, and pollution: aerosol nutrient sources and impacts on ocean biogeochemistry. Ann. Rev. Mar. Sci. 14, 303–330.

Hashihama, F., Yasuda, I., Kumabe, A., Sato, M., Sasaoka, H., Iida, Y., Shiozaki, T., Saito, H., Kanda, J., Furuya, K., Boyd, P.W., Ishii, M., 2021. Nanomolar phosphate supply and its recycling drive net community production in the subtropical North Pacific. Nat. Commun. 12 (1), 3462. https://doi.org/10.1038/s41467-021-23837-y.

Itoh, S., Kaneko, H., Kouketsu, S., Okunishi, T., Tsutsumi, E., Ogawa, H., Yasuda, I., 2021. Vertical eddy diffusivity in the subsurface pycnocline across the Pacific. J. Oceanogr. 77 (2), 185–197.

Johnson, K.S., Riser, S.C., Karl, D.M., 2010. Nitrate supply from deep to near-surface waters of the North Pacific subtropical gyre. Nature 465 (7301), 1062–1065.

Kaneko, H., Yasuda, I., Komatsu, K., Itoh, S., 2013. Observations of vertical turbulent nitrate flux across the Kuroshio. Geophys. Res. Lett. 40 (12), 3123–3127.

Kaneko, H., Yasuda, I., Itoh, S., Ito, S., 2021. Vertical turbulent nitrate flux from direct measurements in the western subarctic and subtropical gyres of the North Pacific. J. Oceanogr. 77 (1), 29–44.

Karl, D.M., Church, M.J., 2017. Ecosystem structure and dynamics in the North Pacific Subtropical Gyre: new views of an old ocean. Ecosystems 20 (3), 433–457.

Laws, E.A., D'Sa, E., Naik, P., 2011. Simple equations to estimate ratios of new or export production to total production from satellite-derived estimates of sea surface temperature and primary production. Limnol. Oceanogr. Meth. 9 (12), 593–601.

Lee, M., Williams, R.G., 2000. The role of eddies in the isopycnic transfer of nutrients and their impact on biological production. J. Mar. Res. 58 (6), 895–917.

Letelier, R.M., Karl, D.M., Abbott, M.R., Bidigare, R.R., 2004. Light driven seasonal patterns of chlorophyll and nitrate in the lower euphotic zone of the North Pacific Subtropical Gyre. Limnol. Oceanogr. 49 (2), 508–519.

Letscher, R.T., Primeau, F., Moore, J.K., 2016. Nutrient budgets in the subtropical ocean gyres dominated by lateral transport. Nat. Geosci. 9 (11), 815–819.

Lewis, M.R., Hebert, D., Harrison, W.G., Platt, T., Oakey, N.S., 1986. Vertical nitrate fluxes in the oligotrophic ocean. Science 234 (4778), 870–873.

Lipschultz, F., Bates, N.R., Carlson, C.A., Hansell, D.A., 2002. New production in the Sargasso Sea: history and current status. Global Biogeochem. Cycles 16 (1), 1001. https://doi.org/10.1029/2000gb001319.

Liu, Z., Lozovatsky, I., 2012. Upper pycnocline turbulence in the northern South China Sea. Chin. Sci. Bull. 57 (18), 2302–2306.

Liu, Z., Lian, Q., Zhang, F., Wang, L., Li, M., Bai, X., Wang, J., Wang, F., 2017. Weak thermocline mixing in the North Pacific low-latitude western boundary current system. Geophys. Res. Lett. 44 (20), 10530–10539.

Luo, L., Kao, S., Bao, H., Xiao, H., Xiao, H., Yao, X., Gao, H., Li, J., Lu, Y., 2018. Sources of reactive nitrogen in marine aerosol over the Northwest Pacific Ocean in spring. Atmos. Chem. Phys. 18 (9), 6207–6222.

Martino, M., Hamilton, D.S., Baker, A.R., Jickells, T., Bromley, T., Nojiri, Y., Quack, B., Boyd, P.W., 2014. Western Pacific atmospheric nutrient deposition fluxes, their impact on surface ocean productivity. Global Biogeochem. Cycles 28 (7), 712–728.

Martiny, A.C., Pham, C.T., Primeau, F., Vrugt, J.A., Moore, J.K., Levin, S.A., Lomas, M. W., 2013. Strong latitudinal patterns in the elemental ratios of marine plankton and organic matter. Nat. Geosci. 6 (4), 279–283.

McDougall, T.J., 1984. The relative roles of diapycnal and isopycnal mixing on subsurface water mass conversion. J. Phys. Oceanogr. 14 (10), 1577–1589.

McDougall, T.J., 1987. Thermobaricity, cabbeling, and water-mass conversion. J. Geophys. Res. 92 (C5), 5448–5464.

Mouriño-Carballido, B., Ferrer, J.L.O., Castro, B.F., Marañón, E., Maseda, M.B., Aguiar-González, B., Chouciño, P., Graña, R., Moreira-Coello, V., Villamaña, M., 2021. Magnitude of nitrate turbulent diffusion in contrasting marine environments. Sci. Rep. 11, 18804. https://doi.org/10.1038/s41598-021-97731-4.

Nagai, T., Durán, G.S., Otero, D.A., Mori, Y., Yoshie, N., Ohgi, K., Hasegawa, D., Nishina, A., Kobari, T., 2019. How the Kuroshio current delivers nutrients to sunlit layers on the continental shelves with aid of near-inertial waves and turbulence. Geophys. Res. Lett. 46 (12), 6726–6735.

Nakamura, Y., Oka, A., 2019. CMIP5 model analysis of future changes in ocean net primary production focusing on differences among individual oceans and models. J. Oceanogr. 75 (5), 441–462.

Oka, E., 2009. Seasonal and interannual variation of North Pacific Subtropical Mode Water in 2003–2006. J. Oceanogr. 65 (2), 151–164.

Omand, M.M., Mahadevan, A., 2013. Large-scale alignment of oceanic nitrate and density. J. Geophys. Res. Oceans 118 (10), 5322–5332.

Osborn, T.R., 1980. Estimates of the local rate of vertical diffusion from dissipation measurements. J. Phys. Oceanogr. 10, 83–89.

Painter, S.C., Patey, M.D., Forryan, A., Torres-Valdés, S., 2013. Evaluating the balance between vertical diffusive nitrate supply and nitrogen fixation with reference to nitrate uptake in the eastern subtropical North Atlantic Ocean. J. Geophys. Res. 118, 5732–5749.

Qi, J., Yu, Y., Yao, X., Yuan, G., Gao, H., 2020. Dry deposition fluxes of inorganic nitrogen and phosphorus in atmospheric aerosols over the Marginal Seas and Northwest Pacific. Atmos. Res. 245, 105076. https://doi.org/10.1016/j.atmosres.2020.105076.

Qu, T., Mitsudera, H., Yamagata, T., 1999. A climatology of the circulation and water mass distribution near the Philippine Coast. J. Phys. Oceanogr. 29 (7), 1488–1505.

Sigman, D.M., Hain, M.P., 2012. The biological productivity of the ocean. Nat. Educ. Knowl. 3 (10), 21. https://eprints.soton.ac.uk/358635/.

Suga, T., Motoki, K., Aoki, Y., Macdonald, A.M., 2004. The North Pacific Climatology of Winter mixed layer and mode waters. J. Phys. Oceanogr. 34 (1), 3–22.

Tanaka, T., Hasegawa, D., Yasuda, I., Tsuji, H., Fujio, S., Goto, Y., Nishioka, J., 2019. Enhanced vertical turbulent nitrate flux in the Kuroshio across the Izu Ridge. J. Oceanogr. 75 (2), 195–203.

Tanioka, T., Garcia, C.A., Larkin, A.A., Garcia, N.S., Fagan, A.J., Martiny, A.C., 2022. Global patterns and predictors of C:N:P in marine ecosystems. Commun. Earth Environ. 3 (1), 271. https://doi.org/10.1038/s43247-022-00603-6.

Tuerena, R.E., Williams, R.G., Mahaffey, C., Vic, C., Green, J.A.M., Naveira-Garabato, A., Forryan, A., Sharples, J., 2019. Internal tides drive nutrient fluxes into the deep chlorophyll maximum over mid-ocean ridges. Global Biogeochem. Cycles 33 (8), 995–1009.

Whalen, C.B., MacKinnon, J.A., Talley, L.D., 2018. Large-scale impacts of the mesoscale environment on mixing from wind-driven internal waves. Nat. Geosci. 11 (11), 842–847.
Yu, X.R., Wen, Z., Jiang, R., Yang, J.-Y.T., Cao, Z., Hong, H., Zhou, Y., Shi, D., 2024. Assessing N_2 fixation flux and its controlling factors in the (sub)tropical western North Pacific through high-resolution observations. Limnol. Oceanogr. Lett. 9 (6), 716–724.
Yuan, Z., Browning, T.J., Zhang, R., Wang, C., Du, C., Wang, Y., Chen, Y., Liu, Z., Liu, X., Shi, D., Dai, M., 2023. Potential drivers and consequences of regional phosphate depletion in the western subtropical North Pacific. Limnol. Oceanogr. Lett. 8 (3), 509–518.